Valorization of calcium hypochlorite precipitate as a new source of heterogeneous catalyst development for biodiesel production: A preliminary experiment

Kedir Derbie Mekonnen [a,*], Kefyalew Hailemariam [b]

[a] School of Mechanical and Chemical Engineering, Kombolcha Institute of Technology-Wollo University, Wollo, Ethiopia
[b] School of Mechanical, Chemical, and Materials Engineering, Adama Science and Technology University, Adama, Ethiopia

ARTICLE INFO

ABSTRACT

One of the main problem related with liquid bleach production from calcium hypochlorite is the amount of precipitates generated and its consequent management. As a result, academic and industrial communities have been challenged with searching of a means for its valorization. Therefore, this research explores the application of the precipitate as a viable source of Ca-based heterogeneous catalyst development for the production of waste cooking oil methyl esters for the first-time. The catalyst was prepared by dividing the precipitates into three forms, viz. raw un-treated (RC), heat treated (RC-TB), and NaOH impregnated plus thermally activated (RC-ITB). The prepared catalysts were efficiently characterized by XRF, XRD, FTIR, SEM, and BET techniques. The characterization results indicated that the catalysts are mainly composed of calcium metal in the form of oxides (CaO), calcite (CaCO$_3$) and Portlandite (Ca(OH)$_2$), which are the promising constituents of basic catalysts. The BET inspection of RC, RC-TB, and RC-ITB revealed the specific surface area of 8.509, 9.089, and 9.312 m^2/g, respectively. At the same reaction conditions, the maximum biodiesel yield of 76.05 % was achieved by RC-ITB compared to RC-TB (62.57 %) and RC (19.74 %), because it's larger specific surface area and highest basic nature (pH = 12.65 at 1:5 w/v) improves the reaction catalysis through better catalyst-substrates interactions. The lower biodiesel yield was attained through the RC catalyst due to its untreated surface, lower specific area, and weak alkaline nature (pH value = 10.66 at 1:5 w/v). Furthermore, regardless of the amount of yield, almost similar fuel properties and functional groups of the products over the coded catalysts were observed. Generally, the possibility of calcium hypochlorite precipitate as a precursor of Ca-based heterogeneous catalyst has been effectively proven in this research, which could be very important for environmental safety and industrial resource integration.

1. Introduction

Globally, energy is renowned as one of the key provisions for socio-economic prosperity. Due to the non-renewable and environmentally dangerous nature of fossil resources, biodiesel as a renewable energy has grown significantly worldwide [1]. However, 70−95 % biodiesel production cost depends on the price of feedstock. One of the low priced source is waste cooking oils mainly palm

---

oil, which considered as a 3rd generation raw material [2]. The fatty acid profile of waste cooking palm oil is reported as linoleic acid (C18:2), lauric acid (C12:0), palmitic acid (C16:0), myristic acid (C14:0), stearic acid (C18:0), and oleic acid (C18:1) [3]. In addition to the selection of cheap raw materials, choosing the right kind of catalyst is very important to reduce the costs of biodiesel synthesis [2, 4]. The three general classes of catalysts used in the *trans*-esterification for biodiesel production are homogenous or heterogeneous, both being acidic or basic. Usually, alkali-homogenous catalyzed reaction system produces high yield of response variable in shorter time under mild reaction conditions when moisture and free fatty acid contents of the feedstock are <0.1 wt% and 0.5 respectively, else acid homogenous catalysts are employed [5–7]. However, homogenous catalysts have several weaknesses such as phase separation difficulty, sensitivity for soap formation at higher FFAs and moisture contents, non-reusability of catalyst thereby increasing waste generation, needs further purification steps such as washing with water to remove the catalyst plus impurities followed by drying which leads to increase wastewater generation and thereby increasing the overall production cost [7–10]. On the other hand, heterogeneous catalysts are solid phases which would not be dissolved in the reactant mixture and could be a noble alternative for homogeneous catalysts in the biodiesel production scenarios [11].

The most impressive significance of heterogeneous catalysts are ease separation, elimination of the washing requirement, reusability, less corrosion problems plus environmental risks, and simultaneously catalyze *trans*-esterification and esterification reactions that can avoid the pre-esterification step for those feed stocks having high free fatty acid contents [5,9,11]; hence, solid catalysts are expected to be used as a good alternative one in the near future due to environmental and economic reasons. But, alkaline solid catalysts are typically superior to solid acids for a variety of reasons; solid acid catalysts react slowly, require high catalyst load, higher temperatures, and higher alcohol reactant requirements compared to the alkali heterogeneous catalysts. As a result, many scholars are involved in research to develop a solid basic catalysts from the various agricultural and industrial wastes [11,12]. The most likely candidate catalysts used in the *trans*-esterification reaction are MgO and CaO, either in neat or modified forms. However, their activity is comparatively slower than homogenous catalysts (KOH and NaOH) as it needs more time to complete the reaction. To overcome this problem, the catalysts are commonly doped with KOH or NaOH for which OH ions can be loaded on the porous structure thus accelerating the rate of methyl ester synthesis [7,13]. Consequently, supported catalysts have better catalytic activity than unsupported ones. Furthermore, upon the combustion of the catalyst sources, the content of organic substances will abruptly decrease, leaving the alkali metal oxides as the main active constituents in the ashes. The occurrence of high-basic-strength oxides in the ashes increased their catalytic ability to produce biodiesel [14].

Currently, the development of alkaline heterogeneous catalysts, typically the Ca-based ones, from various waste materials mostly contained $CaCO_3$ is the interesting topic of many studies increasingly today. Because, catalysts is derived from such like materials have high alkalinity and large amount of feed stocks, for instance waste eggshells, cement-based wastes, bones, etc., which can give CaO with different catalytic activities [10,15,16]. As a result, precipitates of commercial liquid bleaching agent production from calcium hypochlorite are identified as another source of Ca-based catalyst development as part of this research. Calcium hypochlorite is an inorganic compound with the chemical formula $Ca(ClO)_2$, which is being effectively utilized as the active ingredient of bleaching agent to remove the coloring matters and improve the whiteness of things to be bleached [17–21]. However, the bleaching agent processing produces a Ca-rich precipitate that could be used for the development of alternative heterogeneous catalysts instead of its disposal. Uncontrolled disposal of such a precipitate may lead to environment and human health problems because of its corrosive and hazardous properties [19,21]. Even though the precipitate is known to be dangerous, its composition and utilization is not identified until now. Therefore, the objective of this research is limited to know the main chemical constituents of the precipitate and verify its valorization for waste cooking oil methyl esters production as a solid catalyst in triple forms, viz. untreated, thermally treated, and both alkaline plus thermally treated. Consequently, the use of these industrial waste materials as a precursors for heterogeneous catalyst preparation is not only significant for resource integration upon the new insights of this study, but also crucial for environmental safety.

2. Materials and methods

2.1. Materials

The main raw materials, waste cooking palm oil and the precipitates of calcium hypochlorite-based liquid bleach, were respectively collected from local pan-frying chips sellers and robi detergent soap factory, kombolcha, Ethiopia. All chemicals, and Equipments list used throughout this work are presented in the Supplementary Information.

2.2. Methods

2.2.1. FFA and SV of waste cooking oil

The collected crude waste cooking oil (WCO) was first heated to 90 ^{O}C for 1 h to facilitate the removal of solid impurities via filtration [22,23]. Afterward, it was stored in a clean sealed vessel for further usage. The Free fatty acid level and saponification value of WCO were determined by following ASTM D-664 and AOAC, 1990 standard procedures, respectively. Based on these values, the average molecular weight of WCO was predicted empirically with Equation (1) [22].

$$MW_{,wco} = \frac{168,300}{SV - AV} \tag{1}$$

To prove the suitability of the feed stock for homogeneous catalyzed reaction system, WCO was subjected for *trans*-esterification

reaction in the presence of NaOH, as presented on the supporting information (Fig. S1).

2.2.2. Drying and activation of the precipitate

The collected precipitate has a semi-solid state due to the water soaking periods, and hence, it was dried in open air for 4 days to evaporate many of the absorbed water followed by drying in oven at 110 ^{O}C for 3h, and powdered with mortar to a particle size of below 355 μm [10,22,24]. For activation and catalytic evaluation purpose, oven dried samples were prepared and coded with three forms, i.e. untreated raw dried precipitate (RC), thermally activated (RC-TB), and NaOH-impregnated plus thermally activated (RC-ITB). RC-TB was prepared by treating the sample at a calcination condition of 600 ^{O}C for 3 h whereas, the wet impregnation method was implemented for RC-ITB to load OH ions on its porous structure desirable to accelerate the rate of methyl ester synthesis [7,13]. Alkaline impregnation was made by considering 10 g of powder sample suspended with 100 ml distilled water followed by adding 10 ml of 20 % (w/v) NaOH solution and continuously mixed for 2 h impregnation time. Then, the slurry was dried in oven for 16 h at 120 ^{O}C followed by calcination at same condition with RC-TB. The calcination condition plays a significant role in the development of the surface morphology of the catalyst by removing organic substances (volatile matters) and liberating physically absorbed moisture from the surface. Finally, the samples were cooled in a desiccator followed by packing with polyethylene bag to avoid any adsorption of moisture and other contaminants on the surface until further use [7,9,14,22]. All the above procedures are presented in supplementary information (Figs. S2 and S3).

2.2.3. Catalyst characterization

Once the precipitate was prepared and coded with three parts, their properties were characterized. The surface functional group of the catalysts before and after reactions were analyzed via FT-IR (JASCO FT/IR-6600) with the conventional KBr technique from a wave numbers of 400–4000 cm^{-1} at a resolution of 4 cm^{-1} with scanning speed of 2 mm/s because of the transmission of infrared radiation.

The specific surface area of the catalysts were examined by Brunauer–Emmett–Teller (BET) method using SA-9600 series surface area analyzer, Horiba Instruments, USA. The samples were first degassed at 150 ^{O}C for 1h through the analyzer degassing step, and then, a liquid form of nitrogen was adsorbed by the catalyst keeping the bath at 77 K to generate a linear BET curve.

The phase identifications of the catalysts were performed by X-ray diffractometer (XRD-7000, Shimadzu corporation, Japan), at a measuring condition of voltage of 40 kV and current of 30 mA with Cu Kα radiation (λ = 0.154 nm) at a continuous scanning speed of 3°/min. Then, the X-ray detector collects diffracted X-ray patterns rotating at an angle of 2θ in the range of 10 to 80°. The crystalline phases present on the samples were determined by comparing the peak values of 2θ with standards using the match! Software.

The surface morphological characteristics of all the coded catalysts before and after reaction were examined using scanning electron microscope (JCM-6000Plus) operated at acceleration voltage of 15 kV to observe the surface microstructure. For better microstructural implications, SEM analysis of laboratory reagent CaO catalyst, rankem brand, coded with PC was implemented.

To detect major and trace elements of the catalyst, X-ray fluorescence (Thermo scientific Niton XL3t) analysis was performed. But, due to the financial reasons and insensitivity to Na detection, only RC-ITB was subjected for XRF analysis. The machine only detects elements above magnesium ($^{24}_{12}Mg$). Thus, the powder sample was added in a clean cylindrical tube covered with thin film for X-Ray fluorescence transmission; then, its composition was detected by irradiating the sample with X-rays through the film. To detect the contents of sodium ($^{23}_{11}Na$), atomic spectrometer instrument was used by following the wet digestion technique using HClO$_4$, HNO$_3$, and H$_2$O$_2$. Once the Na content was known, the elemental percentage composition into their corresponding oxide forms were converted using the conversion factor of each element.
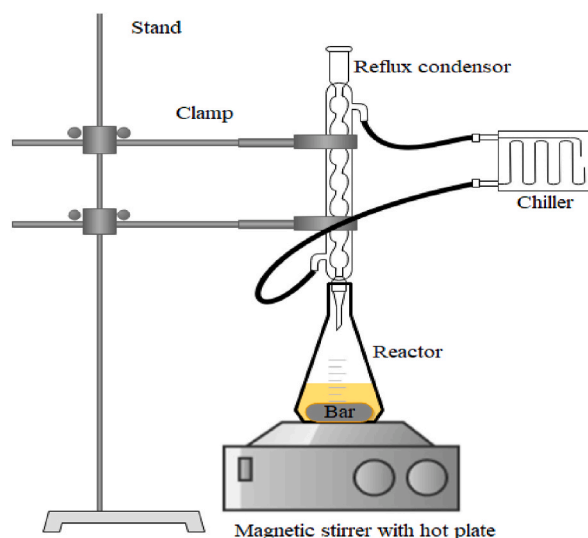

Fig. 1. Experimental setup.

The pH value assessments of the RC, RC-TB, and RC-ITB catalysts were executed by preparing six different dissolution ratio protocols for 1g catalyst in distilled water, viz. 1:5, 1:10, 1:15, 1:20, 1:30 and 1:40 w/v [25,26]. First, the solid-liquid mixture of each protocol was stirred for few minutes, and subsequently test the pH value using digital pH meter (PHS–3C).

2.2.4. Catalytic activity test

The catalytic activity of RC, RC-TB, and RC-ITB were tested on the *trans*-esterification of WCO in the presence of methanol reactant in triplicate experimental confirmations for each catalyst. In this experiment, the reactions were conducted at same conditions for all catalyst types; reaction temperature 60 °C, methanol to oil molar ratio 20, catalyst loading 6 wt%, reaction time 1h, and mixing intensity 600 rpm. The reaction follows four procedures: chemical reaction in the presence of catalyst, separating the solid catalyst with centrifuge, phase separation (glycerin at bottom and biodiesel at top), and removal of unreacted methanol. The reactions were performed in a 250 ml Erlenmeyer flask equipped with reflux condenser as shown in Fig. 1. The heating and mixing were provided by the hot plate with magnetic stirring in presence of magnetic stir bar. For good catalysis, the catalyst with methanol was first stirred in the reactor at 400 rpm for 30 min, the WCO was heated at the desired reaction temperature in a separate flask. Then, the heated oil was added into the reactor. The reactions were performed at increased rpm of 600 and reaction period of 1 h. At the end of reactions, the mixture was separated with WKM centrifuge machine at 3500 rpm, and the supernatant was allowed to settle for 12 h in funnel until two phases/layers were formed, i.e., biodiesel at the top and glycerol at the bottom. Then after, unreacted methanol from the top layer was separated by rotary evaporator (rotavap) followed by drying in oven at 110 °C aiming to remove any moisture and trace methanol if any. The yield of biodiesel from the reaction system combination were calculated by Equation (2).

$$\% \text{ Biodiesel yield, Y} = \frac{\textbf{gram of} \text{produced } \textbf{biodiesel}}{\textbf{gram of WCO} \text{used } \textbf{for the reaction}} * 100 \% \tag{2}$$

The biodiesel yield over the RC, RC-TB, and RC-ITB catalysts were coded by WF: RC, WF: RC-TB, and WF: RC-ITB, respectively.

2.2.5. Fuel property and FT-IR analysis of biodiesel

The fuel properties of biodiesel produced by the three coded catalysts were analyzed by following standard procedures: Acid Value (ASTM D 664), density (ASTM D1298), Cetane number (ASTM D4737), Saponification Value (AOAC, 1990), Pour Point (ASTM D5853), Cloud point (ASTM D 2500), and kinematic viscosity (ASTM D 445).

FT-IR analysis of biodiesel products were performed to check the functional transformations on the products (WF: RC, WF:RC-TB, and WF:RC-ITB) from the starting material, WCO, due to trans esterification reaction. The analysis were done using the transmission mode JASCO FTIR-6600, by sandwiched the liquid samples between two well-polished KBr disks. The IR data's were recorded from a wave numbers of 400–4000 cm^{-1} with a resolution of 4 cm^{-1} and 2 mm/s scanning speed.

3. Results and discussion

3.1. Free fatty acid and saponification value of WCO

Free fatty acid is an important parameter which used to identify biodiesel production process, either homogeneous or heterogeneous catalysis system. To follow homogeneous catalysis, the maximum FFA level of feed stalk is recommended to be less than 2.5 %, otherwise high FFA value causes formation of soap and decrease methyl ester yield [4,27]. However, the FFA value of WCO was about
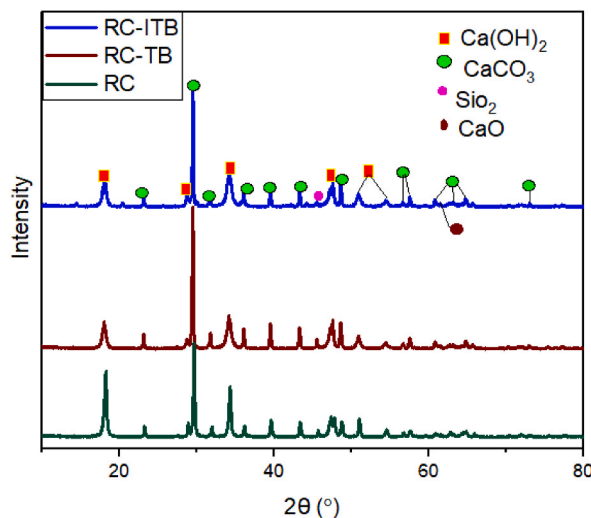

Fig. 2. XRD patterns of RC,RC-TB, and RC-ITB.

16.315 %, and reasonable to use heterogeneous catalysts instead of the homogeneous one. The saponification value of the WCO was 223.4037 mg KOH/g which is slightly greater than the recommended value of vast biodiesel feed stocks (130–193 mg KOH/g). The higher SV denotes the presence of lower molecular weight fatty acids, and its suitability for soap production [28–30]. As a matter of test, WCO was subjected for methyl ester synthesis with NaOH homogeneous catalyst and the result was solid soap.

3.2. Catalyst characterization

3.2.1. XRD analysis

The phase identification of the catalysts (RC,RC-TB, RC-ITB) were confirmed through the use of XRD analysis based on the position of the 2θ diffraction angle varying from 10 to 80°. The position of 2θ is related with some spacing between the atoms or crystals within the sample to be analyzed, obtained by the diffraction angle of the incident X-ray beam sent to the sample. The amount of molecules within that spacing or in that phase is related with the intensity of the peaks; the greater the intensity of the peak, the more molecules or crystals amount in that space. The crystal size is inversely proportional with the width of the peaks. A thinner peak corresponds to the larger crystal, whereas the broader peak resembles a smaller crystal, presence of defect, or it might be naturally amorphous (a solid lacking perfect crystallinity). From Fig. 2, the prominent candidate phases related to the clear diffraction peaks of XRD patterns were identified through the Match! Software. Consequently, the calcite phase ($CaCO_3$) was detected at $2\theta = 23.2^O$, 29.52^O, 31.84^O, 36.1^O, 39.52^O, 43.32^O, 48.62^O, 56.69^O, 57.54^O, 60.8^O, 63.2^O, 64.8^O and 73.02^O. Portlandite ($Ca(OH)_2$) at $2\theta = 18.12^O$, 28.76^O, 34.24^O, 47.66^O, 50.94^O, and 54.52^O. The SiO_2 and CaO phases are distinguished at 2θ value of 45.56^O, and 61.46^O respectively. From the

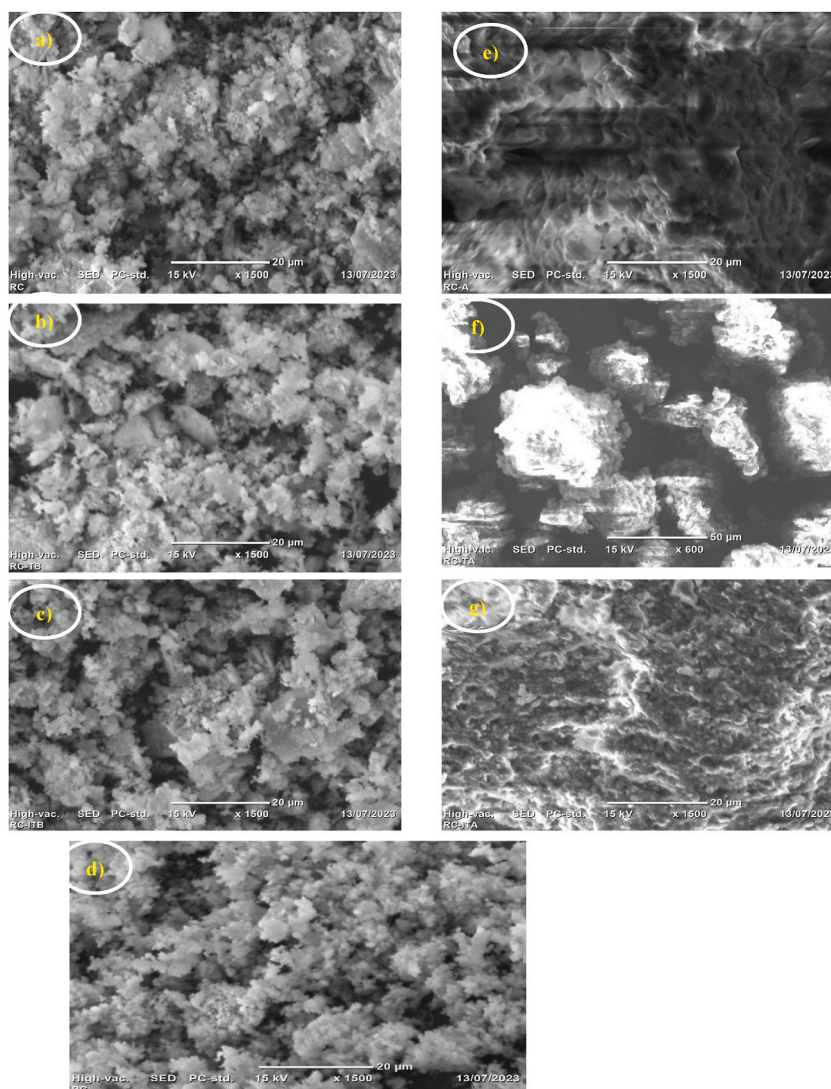**Fig. 3.** SEM images of RC (a), RC-TB (b),RC-ITB (c),PC(d),RC-A (e),RC-TA (f),RC-ITA (g).

diffraction peaks observation, the formation of higher stable polymorph of calcite and Portlandite were observed due to the interaction of combustion products with atmospheric CO_2 and ambient moisture through carbonation and/or hydroxylation, respectively [1,31]. Furthermore, incomplete combustion of the material at a lower temperature might lead to "not much difference between the precursor and the calcined products"; if this is the case, the following alternative auxiliary reactants and reactions can be expected/predicted from the bleach production systems although their formulations were secured. Heuristically, sodium carbonate (Na_2CO_3, soda Ash) or caustic soda (NaOH) could be used in the household bleach processing. Thus,

- If Na_2CO_3 is a reactant: $Ca(OCl)_2 + Na_2CO_3 \rightarrow CaCO_3$(precipitate) $+ 2NaOCl$ (bleach),

  Or.

- If NaOH used: $Ca(OCl)_2 + 2NaOH \rightarrow Ca(OH)_2$ (precipitate) $+ 2NaOCl$ (bleach)

From such mechanisms, it can be noted that either of $CaCO_3$ or $Ca(OH)_2$ was detected because of the precipitation from the bleach processing, and the other one is occurred due to environmental conditions plus lower calcination temperature. Generally, the XRD patterns support all the above inferences. Except the calcite and Portlandite phases, the absence of a perfect diffraction peaks related to the rest of elements identified by the XRF analysis and NaOH impregnation is possibly due to the quantitative insensitivity of XRD machine or their amorphous/homogeneous nature. As a result, they are all detected at the very low and noisy intensities with a zero figure-of-merit (FoM) values of the candidate entries as confirmed in the peak Match software; FoM is the numerical value indicating the degree of agreement between the sample and the standard material diffraction data.

3.2.2. SEM analysis

Scanning electron microscopy is a powerful technique for imaging the surface morphology and microstructure of materials. SEM images are obtained by scanning a focused beam of electrons across a sample and detecting the secondary electrons emitted from the surface. The intensity of the secondary electrons depends on the topography, composition and orientation of the sample, which can reveal valuable information about its behavior. Thus, to extract meaningful insights from the SEM images, the variations of surface structural characteristics, such as shape and patterns of all catalysts with their after reaction phases as well as the reference laboratory reagent CaO micrographs were analyzed as depicted in Fig. 3. From the SEM pictures view, the orientation of the reference catalyst CaO in Fig. 3c shows the various well fashioned lump of fogs like arrangements, implying its porous crystalline structure desirable to offer better active sites for the reaction to happen [7,32]. Because of the presence of surface impurities on the RC catalyst (Fig. 3a) and occurrence of agglomerations in RC-TB (Fig. 3b), the surface characteristics of RC-ITB (Fig. 3c) is more likely seems to the reference catalyst (Fig. 3d) due to the combined alkali-thermal treatments essential to increase its catalytic ability. Furthermore, the bright particles on the SEM image infers the presence of oxygenated matters on the catalyst surface which could be linked with oxides of metals [33]. The micrographs presented in Fig. 3e–g are the surface property of the respective coded catalysts after reaction, and the
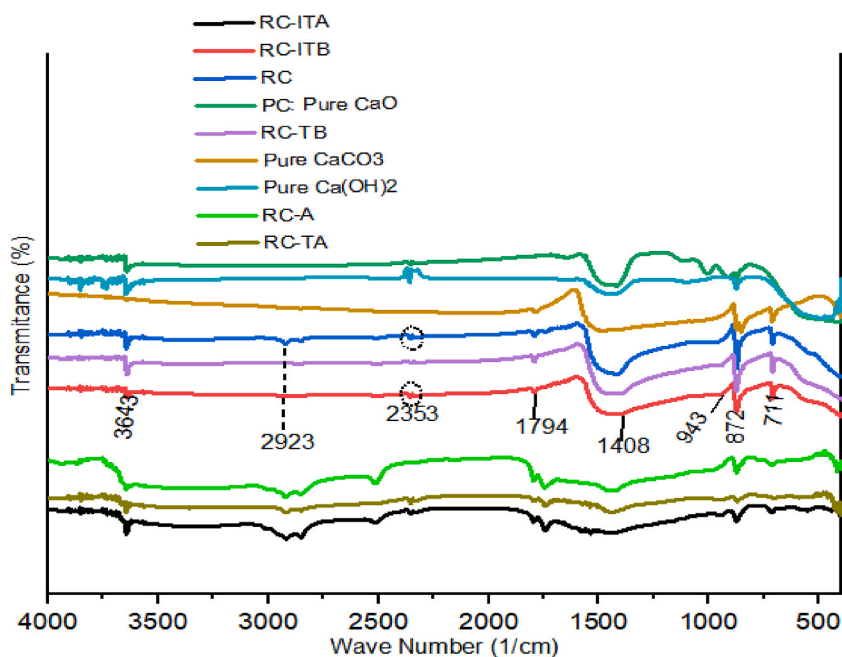

Fig. 4. FTIR spectrum of catalysts.

results remarkably shows the loss of their original structural microporosity. This may possibly due to the accumulation of organic impurities on the surface of the catalyst during the reaction process, which responsible for blocking their active sits [34]. Note that the scanning of RC-TA was done at 50 μm to enhance its visibility, because SEM analysis is affected by the magnification and resolution of the image which determine the level of detail and/or accuracy of certain features.

3.2.3. FTIR analysis

The surface functional groups of the RC,RC-TB, RC-ITB catalysts and their corresponding after reaction phases coded with RC-A, RC-TA, and RC-ITA were confirmed by transmission mode FTIR spectroscopy. For the beset of interpretation, FTIR spectra of Rankem brand laboratory reagents, viz. CaO, $CaCO_3$, and $Ca(OH)_2$ were plotted in combination with them. As proven in Fig. 4, the FTIR patterns of RC,RC-TB, and RC-ITB are almost similar, except the presence of very weak O–H stretching vibration at 2923 cm^{-1} on the RC catalyst due to the presence of the free/unbounded water molecules on the surface, which may be persisted during the leaching of bleach processing from the crystalline hypochlorite; the absence of this band on the RC-TB and RC-ITB catalysts could be reasonably removed by the calcination temperature due to its poorer surface attachments. Moreover, the effect of impregnation on the RC-ITB was detected at 2323 cm^{-1} by developing a new strong chemisorbed O–H bond which are not detached at the prescribed heat treatment, however removal of this bond from the RC surface is reasonably possible due to the physisorbed nature as verified on the RC-TB one. As a matter of degree of agreement with the reference/pure chemical spectra, all the three coded catalysts were in the order with $CaCO_3 >$ $Ca(OH)_2 >$ CaO with some exceptional differences. The band assignments at 3643 and 1794 cm^{-1} is assigned to the O–H bond, because of the absorption of hydroxyl/water molecules adhered to the particle surface to form $Ca(OH)_2$ [1,35]. The band at 1408 cm^{-1} denotes asymmetric C–O bond stretching vibrations of carbonate ions/groups (CO_3^{2-}), which formed due to the chemisorption of atmospheric CO_2 over the catalyst surface. Also, 711 and 872 cm^{-1} indicates the in-plane and out of plane bending vibration of symmetrical C–O bond stretching in the carbonate groups, respectively [1,7,9,31,36]. The peak at 943 cm^{-1} attributed to the Si–O bond due to the presence of silicon dioxide,SiO_2 [1]. All of the above listed compounds were nicely confirmed with XRD and XRF analysis. Furthermore, the deposition of oil derived organic species on the surface of the catalysts during reaction system results shifting of FTIR patterns on the after reaction catalysts (RC-A, RC-TA, and RC-ITA) from their original shapes.

3.2.4. BET analysis

The results of Brunauer-Emmett-Teller surface area analysis for RC, RC-TB, and RC-ITB were 8.509 m^2/g, 9.089 m^2/g, and 9.312 m^2/g, respectively. The results exhibited that the alkaline infused one has larger specific surface area important for better catalyst-oil interactions on its active sits.

3.2.5. Determination of pH value

Fig. 5 shows the observed changes in pH values of the coded catalysts when dissolved in different volumes of distilled water. The results indicated that gradual reduction of pH values with an increase of solvent volume were perceived in all samples, i.e. from 10.66 to 9.83 (RC), 11.97 to 11.21 (RC-TB), and 12.65 to 11.92 (RC-ITB); because, dissolving fixed quantity of alkaline solute in a series incremental volume of water solvent is responsible for neutralization thereby decreasing its pH levels. At the same volume of water, the pH value of RC-ITB is higher than RC and RC-TB, which reasonably caused by the alkaline impregnation liable to increase its basic nature.
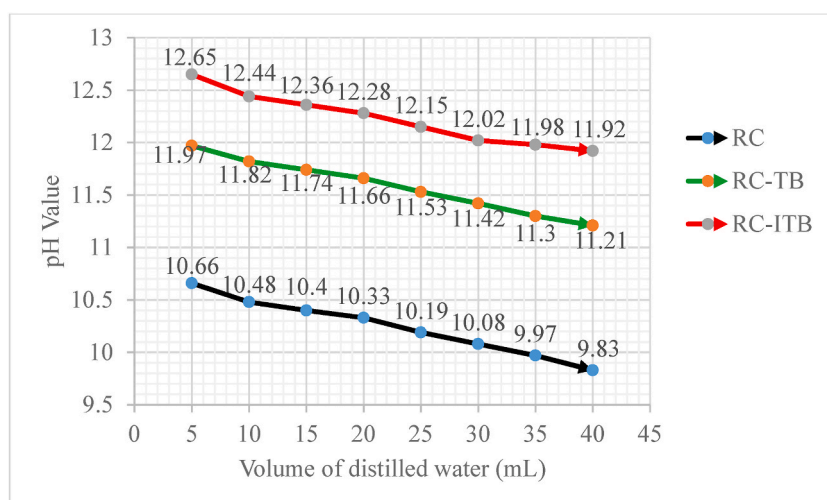

Fig. 5. Deviation of pH value of catalysts (1 g) dissolved in various levels of water.

3.2.6. XRF analysis of RC-ITB

The result of XRF analysis is shown in Table 1 in terms of both elemental and oxide form percentage compositions. The maximum percentage composition of RC-ITB was held by Ca which could be a significant contribution to the Ca-based heterogeneous catalysts development, CaO. Also, a bit of other metallic elements which commonly known to be the active materials for *trans*-esterification reaction were detected along with their oxide forms. The presence of basic oxides improve the basic strength of the catalyst, whereas the acidic components facilitate esterification of the FFA content of feedstock's [37].

3.3. Catalytic activity test

The activities of RC, RC-TB, and RC-ITB catalysts for the synthesis of biodiesel from waste cooking palm oil were confirmed in a triplicate trial experiments for all catalysts as shown in Fig. 6. The results showed that the average FAME yield through RC-ITB catalyst (76.05 %) is higher than RC (19.74 %) and RC-TB (62.57 %). This is due to the fact that alkaline supported catalysts have enhanced basic strength and good catalytic activity to effect high in response variables being produced. In addition, the larger specific surface area of RC-ITB helps to enhance the desired product. A very low biodiesel yield was attained with the RC catalyst because of its untreated surface with lower specific area.

Furthermore, summary of the present study results with other researchers work is presented in Table 2. It is known that every heterogeneous catalysts have their own unique precursor, which responsible for affecting the behavior of the catalyst to be prepared. As a result, the composition and activation conditions of the catalyst sources are obviously determine the quality and catalytic activity of solid catalysts, which in turn to deviate the response variable being produced [15]. The aim of activation is to isolate the desired component by removing the undesired one or loading a new extra components through treatments with thermal, chemical, or a combination of them. Thus, the results of the present study implies that the FAME yield over RC-ITB is comparable with other researchers' findings. The variation between the tabulated values could be directly linked with the type of oil feedstock, levels of reaction conditions used and their optimization, nature of catalyst precursor and activation mode, and particle size. Therefore, precipitates retained from the chemical reaction of calcium hypochlorite with auxiliary alkaline for the production of liquid bleach is interestingly proven as precursors for basic catalyst preparation, which have environmental benefits as well.

3.3.1. Mechanism of heterogeneous catalyzed transesterification reaction

Hypothetically, *trans*-esterification is a chemical process in which biodiesel is produced by reacting 1 mol of triglycerides with 3 mol of short-chain monohydric alcohols, mostly with methanol owing to its quick reactivity, in the presence of catalyst. In this process, the glycerin backbone of the oil molecules are cracked to make mono-alkyl esters, biodiesel (Scheme 1). The overall Transesterification process is normally the sum of three consecutive step reactions which are reversible in nature.

(i) Transformation of triglycerides (TG) to Di-glycerides (DG).
(ii) Di-glycerides to Mono-glycerides (MG).
(iii) Mono-glycerides to mono-alkyl esters (biodiesel) and glycerol

In this study, the pH measurements verified that the prepared solid materials are logically basic which contains mainly a combination of some inorganic bases like CaO, $CaCO_3$, $Ca(OH)_2$, K_2O, Na_2O, and other trace components as identified in XRF and XRD analysis. Thus, the reaction is supposed to be a base catalyzed Transesterification process, for which the catalyst active species and methanol interaction produces nucleophilic methoxide ion [25,39]. Based on this clue, the chemical activity of the catalyst occurring in the Transesterification process was proposed by plausible mechanism (Scheme 2). In the first step, the basic active site/species of the catalyst Z–O (CaO, $CaCO_3$, $Ca(OH)_2$, K_2O, or Na_2O) is interacted with triglyceride molecule and got adsorbed on the surface of catalyst's. Afterward, the surface interaction of the adsorbed triglyceride with methanol results formation of biodiesel (methyl esters) through the nucleophilic attack of the methoxide ion, which is assumed to be released quickly from the catalyst surface. In the last step, the remaining catalyst-glycerol complex is separated by detaching the H-atom from the backbone of catalyst basic species and reconnected to the adsorbed glycerol moiety internally; this results desorption of glycerol molecule from the surface as by-product and the catalyst is reused or recycled via regeneration of active sites.

Table 1
Major elemental and oxide form percentage composition of RC-ITB using XRF.

| Major Elements		Major oxides		Nature
Name	%	Name	%	
Ca	64.26649	Calcium Oxide, CaO	89.9173	Basic
Si	3.015	Silicon dioxide, SiO_2	6.450225	Acidic
Al	1.032	Aluminum Oxide, Al_2O_3	1.949962	Amphoteric
Fe	0.1	Ferric oxide, Fe_2O_3	0.142976	Amphoteric
K	0.08	Potassium oxide, K_2O	0.096368998	Basic
P	0.000435	Phosphorus Pentoxide, P_2O_5	0.000997	Acidic
Na (*detected with AAS*)	0.153875	Sodium Oxide, Na_2O	0.215255	Basic
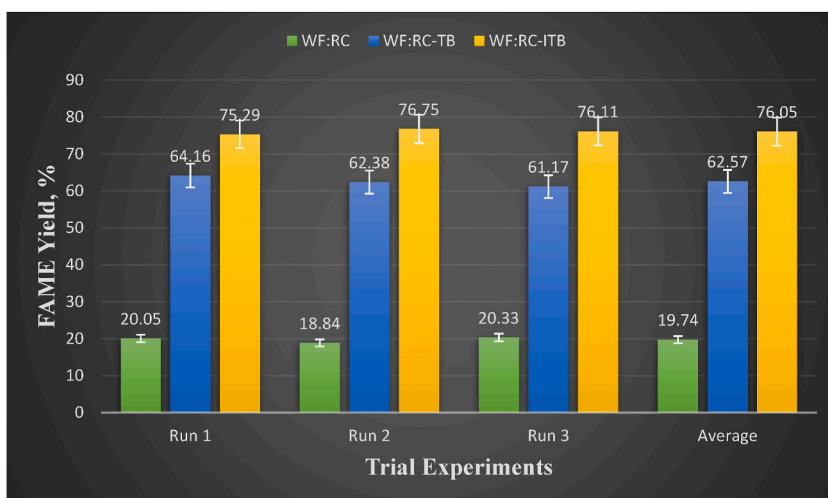
**Fig. 6.** Percentage yields of FAME using the three coded catalysts.

Table 2
Summary of the obtained FAME results in comparison to other reported solid catalysis.

Feedstock	Type of catalyst	Activation Temperature and time, (^{O}C, h)	Method	FAME yield, %	References
Refined coconut oil	OH-impregnated CaO	(600, 2)	Methanolysis with Co-solvent	81.70	[7]
Palm oil	CaO from magnetic-derived CaCO$_3$	-(magnetically treated)	Methanolysis	85	[15]
Waste Frying Oil Valorization	KNO$_3$-Loaded Coffee Husk Ash	(600, 2)	Methanolysis	72.04	[22]
Blend of waste cooking oil and refined palm oil	Fly ash	(120, 2)	Methanolysis	73.8	[1]
canola oil	NaOH loaded sepiolite	(500, 5)	Methanolysis	80.93	[38]
Green alga, Chlorella vulgaris oil	CaO nanocatalyst	(400, 2)	Methanolysis	67	[35]
Waste cooking palm oil	RC	(600, 3)	Methanolysis	19.74	This study
	RC-TB	(600, 3)		62.57	
	RC-ITB	(600, 3)		76.05	
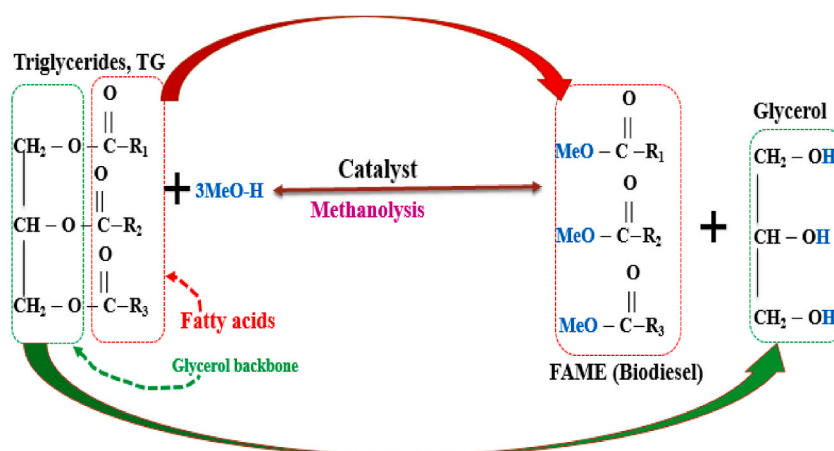
Scheme 1. Overall Transesterification of triglyceride with methanol to biodiesel and glycerol.
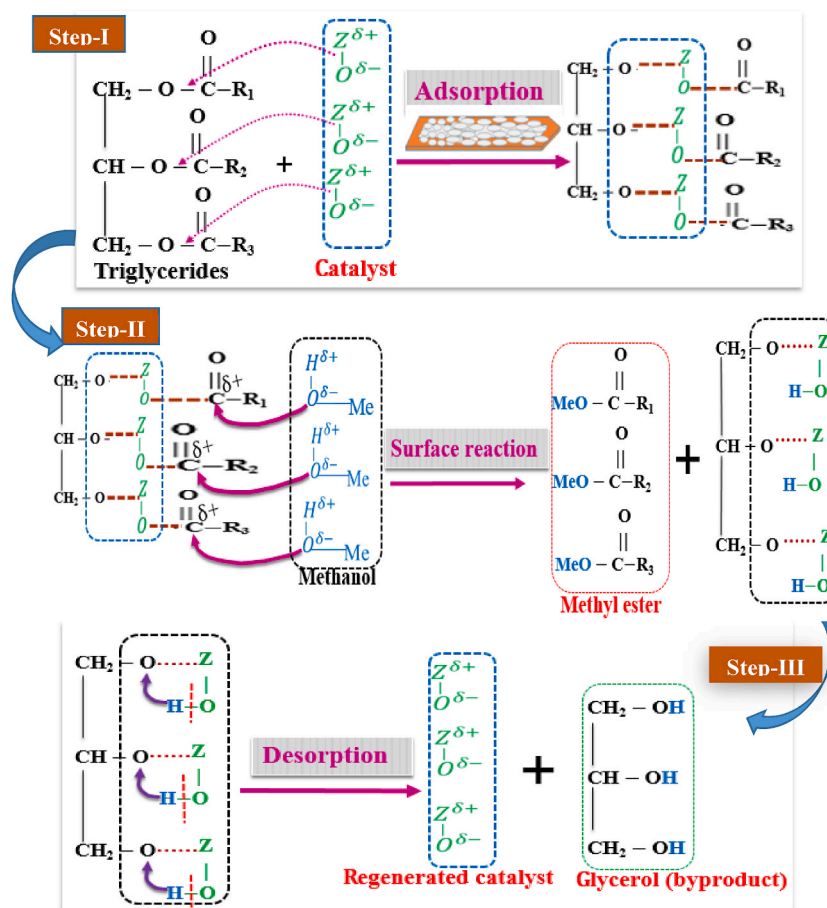
Scheme 2. Plausible mechanism of solid base catalyzed Transesterification on the catalyst surface.

3.4. Fuel property and FT-IR analysis of biodiesel

The fuel properties of WCO derived biodiesels coded with WF: RC, WF: RC-TB, and WF: RC-ITB with respect to the international standard limits are presented in Table 3. Regardless of the amount FAME yield, the fuel properties of the products were nearly similar. The density and kinematic viscosity shows the flow characteristics of the WCO methyl ester. The experimental results of both parameters are within the standard limits. When their values became higher, it needs high injection pressures, unequal distribution, formation of engine deposits, poorer spray, and incomplete combustion could resulted. For better combustion efficiency, blending of

Table 3
Fuel properties of WCO derived FAME over the three catalysts.

Property	unit	Experimental Result	Standard limits	
			Biodiesel	
			ASTM D6751	EN 14,214
Specific gravity@ 15 ^{O}C	–	0.876[a,b,c]	0.87–0.98	–
Density@15 ^{O}C	kg/m^3	875.1[a,b,c]	880 max	860–900
Kinematic Viscosity@40 ^{O}C	mm^2/s	4.91[a];4.93[b];4.94[c]	1.9–6.0	3.5–5.0
Acid Value	mg KOH/g	0.73[a]; 0.76[b];0.78[c]	< 0.8	≤ 0.5
Saponification Value	mg KOH/g	136.72[a]; 137.46[b];140.12[c]	370 max	–
Pour point	^{O}C	−1.33[a]; −1.86[b]; −1.58[c]	−15 to 16	–
Cloud point	^{O}C	4.66[a]; 6.5[b]; 6.88[c]	−3.0 to 12	–
Cetane number	–	30.2[a];32.5[b]; 32.8[c]	≥ 47	≥ 51

Where.
[a] WF:RC-ITB.
[b] WF:RC-TB.
[c] WF:RC products.

biodiesel with the conventional fuels is commonly recommended [4,40].

The acid value and saponification value respectively indicates the corrosive and jelly characteristics of the biodiesel during application. Quantitatively, acid value shows the number of carboxylic acidic groups present in the sample, whereas, saponification value represents milligrams of KOH needed to saponify 1 g of sample [2,41]. Because of the *Trans*-esterification process, their values were reduced well from the starting feed stock, WCO, and satisfactorily within ASTM D6751.

The cloud point and pour point represents the cold flow property of the biodiesel product. The temperature at which smallest crystals or visible wax-like formation due to initiation of molecular "close packing" is termed as cloud point. Whereas, pour point is the temperature at which the fuel loses its flow properties because of larger crystals fused together; therefore the fuel is appropriate for the process just above the pour point [2,42–44]. The experimental values of cloud and pour point are acceptably meet ASTM D6751 standard limit for minimum qualities.

The auto-ignition characteristics of the fuel in a power diesel engine is indicated by cetane number, and it depends on the fuel composition. The higher the CN, the shorter ignition delay (time interval between the start of injection and initiation of ignition) [2,44, 45]. The experimentally determined values of the cetane number are all lower than the standard limits of ASTM D6751 and EN 14,214. This may arise from the presence of unsaturation, and/or high aromatic contents in the biodiesel [45]. Since aniline ($C_6H_5NH_2$) is the simplest aromatic amines, i.e. unsaturated, the sample was completely mixed at the tested ambient temperatures, which imply its aromaticity of the sample to have low aniline point and cetane number.

3.4.1. FT-IR analysis of biodiesel catalyzed over the three catalysts

To confirm the transformation of WCO to the corresponding methyl ester over the RC, RC-TB and RC-ITB catalysts, transmission mode FTIR spectroscopic analysis was implemented. The various molecules present in oils are mainly oxygen-containing functional groups. In FT-IR spectra, the well separated peaks of oils are in the fingerprint region (1500 - 700 cm^{-1}) and between 3100 and 1700 cm^{-1}. However, the peak of 1400 to 600 cm^{-1} in the fingerprint region corresponds with the key bands of methyl esters that make up the biodiesel, because of the C–O bond asymmetric axial deformation. Regardless of being strong or weak bands as depicted in Fig. 7, most of the principal band assignments of WCO with its corresponding FAME products using the three catalysts shared the presence of similar functional groups between them as shown in Table 4. But, there is a clear variation between the WCO and biodiesel products spectra's in the fingerprint region due to the stretching vibration of C–O bond and formation of new functional groups [4]. This reasonably infers the removal of glycerol backbone of triglycerides from the broad convex-like bands, and the unique sharp peak associated with the substitution of methoxyl groups (O–CH$_3$) in the FAME through *trans*-esterification reaction were observed at around 1016 cm^{-1} [4,46]. In addition, the broad band OH-stretching in the WCO which is transformed into somehow straight line in the biodiesel products could be predominantly linked with the acid value of the precursor, and reduced because of the Tran-esterification system.

4. Conclusion

In this study, the precipitates of liquid bleach production from calcium hypochlorite as a viable source of Ca-based solid catalyst for the Transesterification of waste cooking oil to biodiesel have been introduced. Thus, coded catalysts were prepared from the precipitate in three forms, viz. raw untreated (RC), heat treated (RC-TB), and alkaline impregnated plus thermally activated (RC-ITB). The characterization results indicated the presence of higher Ca concentrations in the form of CaO, CaCO$_3$, and Ca(OH)$_2$, which are the prospective components of basic catalysts. Through BET analysis, specific surface area of 8.509, 9.089, and 9.312 m^2/g were confirmed for RC, RC-TB, and RC-ITB, respectively. The basic nature evaluation exhibited that RC-ITB has more alkalinity (pH = 12.65 at 1:5 dilution ratio) mainly due to its OH impregnation. Moreover, the maximum biodiesel yield of 76.05 % was achieved by RC-ITB compared with RC-TB (62.57 %) and RC (19.74 %) at the same reaction conditions, because it's higher alkaline nature and larger specific area plays a significant roles in reaction catalysis. The fuel properties of biodiesel produced over the three coded catalysts were analyzed and acceptably meet ASTM D6751 standard limits for minimum qualities, except the cetane number. Furthermore, the formation of FAME on the biodiesel products due to the substitution of methoxyl group for the cracked glycerol backbone of oil molecules through catalytic Transesterification were attractively inspected using FT-IR spectroscopy. Generally, the results proved that calcium hypochlorite precipitate is the newly source of heterogeneous catalyst development, which could be vital for future industrial resource integration and environmental well-being.

Data availability statement

Data included in article/supp. Material/referenced in article.

CRediT authorship contribution statement

Kedir Derbie Mekonnen: Writing – review & editing, Writing – original draft, Visualization, Validation, Methodology, Investigation, Formal analysis, Data curation, Conceptualization. **Kefyalew Hailemariam:** Writing – review & editing, Validation,
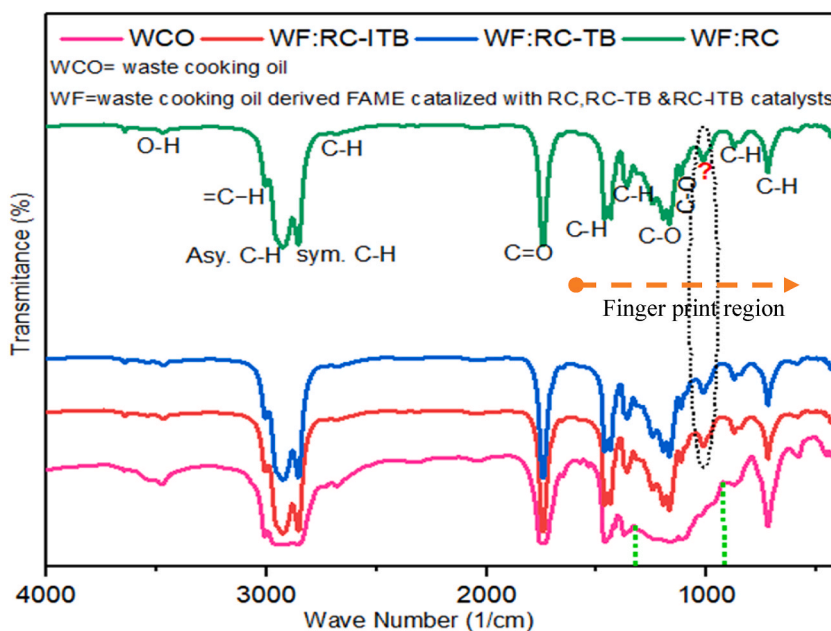
Fig. 7. FT-IR spectra of WCO FAME catalyzed over RC, RC-TB, and RC-ITB catalysts.

Table 4
Main characteristic bands of WCO, WF: RC, WF:RC-TB, and WF:RC-ITB.

∼ wave number, cm^{-1}		Type of Vibration	Functional group
WCO	FAME		
3473	3473	(O–H) stretching	Carboxylic acids and moisture
3006	3006	(=C–H) stretching	Aromatics and Alkenes
2930	2923	(C–H) Asymmetric Stretching	Aliphatics
2844	2854	(C–H) Symmetric Stretching	Aliphatics
2683	2678	C–H Stretching	Aldehyde
1748	1744	(C=O) stretching	Esters, Aldehyde and ketones
1459	1458	(C–H) bending vibration in methylene (–CH$_2$–) & methyl (–CH$_3$–)	Alkane
1374	1362	(C–H) bending vibration in methyl (–CH$_3$–)	Alkane
1168	1168	(C–O) Asymmetric Stretching in C–C(=O)–O bonds	Ester
1112	1115	(C–O) Asymmetric Stretching in O–C–C bonds	Ester
870	874	C–H bending vibration	Aromatics
722	723	C–H rocking vibration	Alkane

Supervision, Resources, Methodology, Investigation, Formal analysis.

Declaration of competing interest

The authors declare no conflict of interest.

Acknowledgements

Appendix A. Supplementary data

Supplementary data to this article can be found online at https://doi.org/10.1016/j.heliyon.2023.e21959.

References

[1] E.M. Vargas, L. Ospina, M.C. Neves, L.A.C. Tarelho, M.I. Nunes, Optimization of FAME production from blends of waste cooking oil and refined palm oil using biomass fly ash as a catalyst, Renew. Energy 163 (2021) 1637–1647, https://doi.org/10.1016/j.renene.2020.10.030.

[2] D. Singh, D. Sharma, S.L. Soni, S. Sharma, D. Kumari, Chemical compositions , properties , and standards for different generation biodiesels : a review, Fuel 253 (2019) 60–71, https://doi.org/10.1016/j.fuel.2019.04.174.

[3] P. Maneechakr, S. Karnjanakom, A combination of 2k factorial with Box-Behnken designs for FAME production via methanolysis of waste cooking palm oil over low-cost catalyst, J. Environ. Chem. Eng. 7 (2019), 103389, https://doi.org/10.1016/j.jece.2019.103389.

[4] K.D. Mekonnen, Z.B. Sendekie, NaOH-catalyzed methanolysis optimization of biodiesel synthesis from desert date seed kernel oil, ACS Omega 6 (2021) 24082–24091, https://doi.org/10.1021/acsomega.1c03546.

[5] D.Y.C. Leung, X. Wu, M.K.H. Leung, A review on biodiesel production using catalyzed transesterification, Appl. Energy 87 (2010) 1083–1095, https://doi.org/10.1016/j.apenergy.2009.10.006.

[6] M. Tariq, S. Ali, N. Khalid, Author ' s personal copy Activity of homogeneous and heterogeneous catalysts , spectroscopic and chromatographic characterization of biodiesel, Review 16 (2012) 6303–6316, https://doi.org/10.1016/j.rser.2012.07.005. Contents.

[7] L.S.H. Dizon, C. Engineering, S. Planning, Biodiesel production from re fi ned coconut oil using hydroxide- impregnated calcium oxide by cosolvent method, Renew. Energy 163 (2021) 571–578, https://doi.org/10.1016/j.renene.2020.08.115.

[8] W. Huang, S. Tang, H. Zhao, S. Tian, Activation of Commercial CaO for Biodiesel Production from Rapeseed Oil Using a Novel Deep Eutectic Solvent, 2013, pp. 11943–11947.

[9] V. Mutreja, S. Singh, A. Ali, Biodiesel from mutton fat using KOH impregnated MgO as heterogeneous catalysts, Renew. Energy 36 (2011) 2253–2258, https://doi.org/10.1016/j.renene.2011.01.019.

[10] Ö. Bedir, T.H. Doğan, Environmental effects comparison of catalytic activities of Ca-based catalysts from waste in biodiesel production, energy sources, Part A: recovery, utilization, and Environmental Effects (2021) 1–18, https://doi.org/10.1080/15567036.2021.1883159.

[11] R. Mat, R.A. Samsudin, M. Mohamed, A. Johari, Solid catalysts and their application in biodiesel production, Bull. Chem. React. Eng. Catal. 7 (2012) 142–149, https://doi.org/10.9767/bcrec.7.2.3047.142-149.

[12] V. Mandari, S. Kumar, Biodiesel production using homogeneous , heterogeneous , and enzyme catalysts via transesterification and esterification reactions : a critical review, BioEnergy Research (2022) 935–961, https://doi.org/10.1007/s12155-021-10333-w.

[13] D.M. Marinkovi, M. V Stankovi, A. V Veli, J.M. Avramovi, M.R. Miladinovi, O.O. Stamenkovi, V.B. Veljkovi, M. Jovanovi, Calcium oxide as a promising heterogeneous catalyst for biodiesel production : current state and perspectives, Renew. Sustain. Energy Rev. 56 (2016) 1387–1408, https://doi.org/10.1016/j.rser.2015.12.007.

[14] S.H.Y.S. Abdullah, N.H.M. Hanapi, A. Azid, R. Umar, H. Juahir, H. Khatoon, A. Endut, A review of biomass-derived heterogeneous catalyst for a sustainable biodiesel production, Renew. Sustain. Energy Rev. 70 (2017) 1040–1051, https://doi.org/10.1016/j.rser.2016.12.008.

[15] C. Sronsri, W. Sittipol, K. U-yen, Performance of CaO catalyst prepared from magnetic-derived CaCO 3 for biodiesel production, Fuel 304 (2021), 121419, https://doi.org/10.1016/j.fuel.2021.121419.

[16] J. Si, J. Ling, Y. Hua, T. Nabisab, M. Mubarak, J. Kansedo, A. Saptoro, C.N. Hipolito, A Review of Heterogeneous Calcium Oxide Based Catalyst from Waste for Biodiesel Synthesis, SN Applied Sciences, 2019, https://doi.org/10.1007/s42452-019-0843-3.

[17] L. Smith, Historical Perspectives on Water Puri Fi Cation, Elsevier Inc., 2017, https://doi.org/10.1016/B978-0-12-809330-6.00012-X.

[18] T. Hussain, Bleaching and Dyeing of Jute, 2016, https://doi.org/10.1016/B978-0-12-803581-8.04080-7.

[19] S.S. Anand, D. Haskell, G. Centers, E. Sciences, Chlorination byproducts, Encyclopedia of Toxicology 1 (2014) 855–859, https://doi.org/10.1016/B978-0-12-386454-3.00276-1.

[20] M. Aamir, N.A. Khan, S. Ahmed, A. Husain, A. Hussain, F. Changani, M. Youse, Chlorination disinfection by-products in municipal drinking water - a review, J. Clean. Prod. 273 (2020), https://doi.org/10.1016/j.jclepro.2020.123159.

[21] X.F. Li, W.A. Mitch, Drinking water disinfection byproducts (DBPs) and human health effects: multidisciplinary challenges and opportunities, Environ. Sci. Technol. 52 (2018) 1681–1689, https://doi.org/10.1021/acs.est.7b05440.

[22] D.T. Bekele, N.T. Shibeshi, A.S. Reshad, KNO3-Loaded coffee husk ash as a heterogeneous alkali catalyst for waste frying oil valorization into biodiesel, ACS Omega 7 (2022) 45129–45143, https://doi.org/10.1021/acsomega.2c05572.

[23] R. Naveenkumar, G. Baskar, Biodiesel production from Calophyllum inophyllum oil using Zinc doped Calcium oxide (Plaster of Paris) nanocatalyst, Bioresour. Technol. 280 (2019) 493–496, https://doi.org/10.1016/j.biortech.2019.02.078.

[24] A.A. Ayoola, O.S.I. Fayomi, I.F. Usoro, Data on PKO biodiesel production using CaO catalyst from Turkey bones, Data Brief 19 (2018) 789–797, https://doi.org/10.1016/j.dib.2018.05.103.

[25] B. Basumatary, B. Das, B. Nath, S. Basumatary, Synthesis and characterization of heterogeneous catalyst from sugarcane bagasse : production of jatropha seed oil methyl esters, Current Research in Green and Sustainable Chemistry 4 (2021), 100082, https://doi.org/10.1016/j.crgsc.2021.100082.

[26] B. Basumatary, S. Basumatary, B. Das, B. Nath, Waste Musa paradisiaca plant : an ef fi cient heterogeneous base catalyst for fast production of biodiesel, J. Clean. Prod. 305 (2021), 127089, https://doi.org/10.1016/j.jclepro.2021.127089.

[27] M. Mo, H.H. Masjuki, M.A. Kalam, A.E. Atabani, Evaluation of biodiesel blending , engine performance and emissions characteristics of Jatropha curcas methyl ester : Malaysian perspective, Energy 55 (2013), https://doi.org/10.1016/j.energy.2013.02.059, 879e887 Contents.

[28] A. Jauro, M.H. Adams, A. Jauro, M.H. Adams, Production and Biodegradability of Biodiesel from Balanites Aegyptiaca Seed Oil, vol. 55, 2016, https://doi.org/10.5012/jkcs.2011.55.4.680.

[29] W. Odoom, V.O. Edusei, Evaluation of saponification value , iodine value and insoluble impurities in coconut oils from jomoro district in the western region of Ghana, Asian Journal of Agriculture and Food Sciences 3 (2015) 494–499.

[30] C.U. Zang, A.A. Jock, H.I. Garba, Y.I. Chindo, Application of desert date (balanites aegyptiaca) seed oil as potential raw material in the formulation of soap and lotion, Am. J. Anal. Chem. 9 (2018) 423–437, https://doi.org/10.4236/ajac.2018.9033.

[31] M. El Bakkari, V. Bindiganavile, Y. Boluk, Facile synthesis of calcium hydroxide nanoparticles onto TEMPO-oxidized cellulose nanofibers for heritage conservation, ACS Omega (2019), https://doi.org/10.1021/acsomega.9b02643.

[32] N.E. Pour, F. Dumeignil, B. Katryniok, L. Delevoye, B. Revel, Investigating the active phase of Ca-based glycerol polymerization catalysts : on the importance of calcium glycerolate, Mol. Catal. 507 (2021), https://doi.org/10.1016/j.mcat.2021.111571.

[33] B. Nath, P. Kalita, B. Das, S. Basumatary, Highly Efficient Renewable Heterogeneous Base Catalyst Derived from Waste Sesamum indicum Plant for Synthesis of Biodiesel, Renewable Energy, 2019, https://doi.org/10.1016/j.renene.2019.11.029.

[34] B.E. Olubunmi, B. Karmakar, O.M. Aderemi, G. A.U, M. Auta, G. Halder, Parametric optimization by Taguchi L9 approach towards biodiesel production from restaurant waste oil using Fe-supported anthill catalyst, J. Environ. Chem. Eng. 8 (2020), 104288, https://doi.org/10.1016/j.jece.2020.104288.

[35] M. Davoodbasha, A. Pugazhendhi, J. Kim, S. Lee, Biodiesel production through transesterification of Chlorella vulgaris : synthesis and characterization of CaO nanocatalyst, Fuel 300 (2021), 121018, https://doi.org/10.1016/j.fuel.2021.121018.

[36] N. Laohavisuti, B. Boonchom, W. Boonmee, Simple Recycling of Biowaste Eggshells to Various Calcium Phosphates for Specific Industries, Nature Publishing Group UK, 2021, https://doi.org/10.1038/s41598-021-94643-1.

[37] T. Ngoya, E.F. Aransiola, O. Oyekola, Optimisation of biodiesel production from waste vegetable oil and eggshell ash, S. Afr. J. Chem. Eng. (2017), https://doi.org/10.1016/j.sajce.2017.05.003.

[38] S. Aslan, N. Aka, M.H. Karaoglu, NaOH impregnated sepiolite based heterogeneous catalyst and its utilization for the production of biodiesel from canola oil, Energy Sources, Part A Recovery, Util. Environ. Eff. 41 (2019) 290–297, https://doi.org/10.1080/15567036.2018.1516010.

[39] S. Basumatary, B. Nath, B. Das, P. Kalita, B. Basumatary, Utilization of renewable and sustainable basic heterogeneous catalyst from Heteropanax fragrans (Kesseru) for effective synthesis of biodiesel from Jatropha curcas oil, Fuel 286 (2021), 119357, https://doi.org/10.1016/j.fuel.2020.119357.

[40] O. Ogunkunle, O.O. Oniya, A.O. Adebayo, Yield response of biodiesel production from heterogeneous and homogeneous catalysis of milk bush seed (thevetia peruviana) oil, Energy and Policy Research 4 (2017) 21–28, https://doi.org/10.1080/23815639.2017.1319772.

[41] R. Kumar, V. Kumar, R. Sham, Stability of biodiesel – a review, Renew. Sustain. Energy Rev. 62 (2016) 866–881, https://doi.org/10.1016/j.rser.2016.05.001.

[42] S.K. Hoekman, A. Broch, C. Robbins, E. Ceniceros, M. Natarajan, Review of biodiesel composition , properties , and specifications, Renew. Sustain. Energy Rev. 16 (2012) 143–169, https://doi.org/10.1016/j.rser.2011.07.143.

[43] R. Naureen, M. Tariq, I. Yusoff, A.J.K. Chowdhury, M.A. Ashraf, Synthesis, spectroscopic and chromatographic studies of sunflower oil biodiesel using optimized base catalyzed methanolysis, Saudi J. Biol. Sci. 22 (2014) 332–339, https://doi.org/10.1016/j.sjbs.2014.11.017.

[44] S. Sani, M.U. Kaisan, D.M. Kulla, A.I. Obi, A. Jibrin, B. Ashok, Industrial Crops & Products Determination of physico chemical properties of biodiesel from Citrullus lanatus seeds oil and diesel blends, Ind. Crops Prod. 122 (2018) 702–708, https://doi.org/10.1016/j.indcrop.2018.06.002.

[45] A. Nalgundwar, B. Paul, S.K. Sharma, Comparison of performance and emissions characteristics of di CI engine fueled with dual biodiesel blends of palm and jatropha, Fuel 173 (2016) 172–179, https://doi.org/10.1016/j.fuel.2016.01.022.

[46] K.D. Mekonnen, Fourier transform infrared spectroscopy as a tool for identifying the unique characteristic bands of lipid in oilseed components: confirmed via Ethiopian indigenous desert date fruit, Heliyon 9 (2023), e14699, https://doi.org/10.1016/j.heliyon.2023.e14699.